



## AN INVESTIGATION OF NUCLEATION AND GROWTH OF MAGNESIUM THIN FILMS PREPARED BY VACUUM DEPOSITION TECHNIQUE.

**B.B. DHALE, K.V. SUKHATANKAR, M.M. BELEKAR AND V.V. BHIDE**

Department of Physics, Gogate Jogalekar College, Ratnagiri. (M.S), India -415612

### ABSTRACT

Magnesium thin films have been deposited on glass and  $\text{Al}_2\text{O}_3$  substrates by vacuum evaporation technique. The films were characterized by scanning electron microscopy, x-Ray diffraction technique and atomic force microscopy measurements. The effect of deposition rate on growth of the magnesium film was studied, the film deposited at deposition rate  $20 \text{ \AA}/\text{sec}$  on glass substrate yields c-axis oriented magnesium films, which shows single peak of (002) for the film grown at  $20 \text{ \AA}/\text{sec}$ . However, the film grown at the deposition rate other than  $20 \text{ \AA}/\text{sec}$  show minor peak of (101) plane. The film grown on  $\text{Al}_2\text{O}_3$  substrates yields films with higher crystallinity which was confirmed by XRD and SEM studies. The optimized deposition rate for growth of magnesium films on  $\text{Al}_2\text{O}_3$  substrates is  $10 \text{ \AA}/\text{s}$ . The improved crystallinity of the film on  $\text{Al}_2\text{O}_3$  substrates is due to crystallinity of  $\text{Al}_2\text{O}_3$  substrates compared to amorphous glass substrate.

**Keywords:** Magnesium thin films, vacuum evaporation technique

### 1.1 INTRODUCTION

The featured properties of superconducting  $\text{MgB}_2$  have created tremendous interest in its thin film synthesis for device applications such as Josephson three terminal electronic devices. Though this intermetallic seems simple binary compound, its synthesis has many hurdles especially in thin film form due to difference in melting point of its components. As an alternative to this, Pawar et.al have synthesized  $\text{MgB}_2$  on conducting (silver) substrate by electrochemical co-deposition at ambient temperature and pressure. However, for electronic application one requires films deposited on non-conducting substrate unlike for high current conductor applications; where one needs conducting substrates. In this situation soft electrochemical process involving deposition of precursor magnesium film on non-conducting substrates like glass, alumina etc. and its subsequent conversion into  $\text{MgB}_2$  by boron intercalation was expected to give success in growing  $\text{MgB}_2$  films on non-conducting substrate. In this paper deposition of

precursor magnesium films by vacuum evaporation technique and its optimization to get good quality pinhole free films is discussed along with nucleation and growth process in vacuum deposition.

### 1.2 Nucleation and growth of the film from vapour phase

Solid material vaporizes when heated to sufficiently high temperatures. The condensation of the vapour onto a cooler substrate yields thin solid films. The deposition by the thermal evaporation method is simple, convenient and is at present the most widely used.

Because of collision with ambient gas atoms, a fraction of the vapour atoms proportional to  $\exp(-d/l)$  will be scattered and hence randomized in direction in a distance 'd' during their transfer through gas. Here 'l' is the mean free path (mfp) of gas atoms, which for air molecules at  $25 \text{ }^\circ\text{C}$  and pressure  $10^{-4}$  and  $10^{-6}$  Torr respectively, is about 45 and 4500 cm. Thus pressure lower than  $10^{-5}$  Torr is necessary to ensure a straight line path for most of the emitted vapour atoms in a vacuum evaporator

for substrate to source distance of ~10 to 50 cm. The rate of free evaporation ( $m_e$ ) of vapour atoms from a clean surface of a unit area in vacuum is given by Langmuir expression,

$$m_e = 5.83 \times 10^{-2} \rho_e (M/T)^{1/2} \text{ gm/cm}^2 \cdot \text{sec} \quad (1.1)$$

Where,  $\rho_e (<10^{-2})$  is the equilibrium vapour pressure (Torr) of evaporant under saturated vapour condition at temperature 'T' and 'M' is the molecular weight of the vapour species. Alternatively, this can be modified to write the evaporation rate as

$$N_e = 3.513 \times 10^{22} \rho_e (1/MT)^{1/2} \text{ molecules/(cm)}^2 \cdot \text{(sec)}. \quad (1.2)$$

However the rate of deposition of the vapour on substrate depends on the source geometry, its position relative to the substrate, and the condensation coefficient. For the ideal case of deposition from a clean uniformly emitting point source on to a plane receiver, the rate of deposition varies as  $\cos\theta/r^2$  (Knudsen cosine law); where r is the radial distance of the receiver from source and  $\theta$  is the angle between the radial vector and normal to the receiver direction.

Thermal evaporation can be achieved directly or indirectly by variety of physical methods. One of the simplest methods is resistive heating. The material is evaporated with a resistively heated filament or boat generally made of refractory metals such as W, Mo, Ta and Nb with or without ceramic coatings. Crucibles of quartz, graphite, alumina, beryllia and zirconia are used with indirect heating. The choice of support material is primarily, determined by evaporation technique and resistance to alloying and / or chemical reaction with evaporant. With the exceptions of highly reactive materials such as Si, Al, Co, Fe and Ni most materials present no problem with evaporation from suitable support [1].

Once the material of interest is vaporized from source with the particular evaporation technique, the condensation of atoms from vapor phase onto a cooler substrate yields thin solid film. Generally there are three steps involved in the film deposition, viz Condensation, Nucleation and Growth.

Atomic condensation takes place in the form of three dimensional nuclei which then grow to

form continuous film by diffusion control process [2,3,4]. The condensation process involves the interaction between vapor atom and the impinging surface. The vapor atom is attracted by the substrate surface by the instantaneous dipole and quadrupole moments of the surface atoms. As a result the atom loses its velocity component normal to the surface in a short time. The vapour atom is then physically adsorbed, termed as adatom. It may move over the surface by jumping from one potential well to the other because of the thermal activation from surface and or its own kinetic energy parallel to surface. The adatom has finite residence time on the substrate surface during which it may interact with other adatom to form stable cluster and chemisorbed or incorporated into surface with release of heat of condensation. If not adsorbed the adatom evaporates into vapor phase [1]. The probability that an impinging atom will be incorporated into the substrate is called the condensation or sticking coefficient. According to famous Langmuir-Frenkel theory of condensation [5,6], the adsorbed atoms move over the surface during their lifetime to form pairs which intern acts as condensation centers for the other atoms. This cluster or subcritical nuclei are formed by collisions of adatoms on the substrate surface [7-11] and in vapor phase if supersaturation is sufficiently high, they continue to grow with increase in free energy until critical size is reached above which growth continues with a decrease in free energy. The Gibbs free energy for the formation of spherical cluster of radius 'r' is given by sum of surface energy to create the surface & volume energy of condensation,

$$\Delta G_0 = 4\pi r^2 \sigma_{cv} + 4/3\pi r^3 \Delta G_v \quad (1.3)$$

Where  $\sigma_{cv}$  is the condensate vapor interfacial free energy &  $\Delta G_v = (kT/V)$  is the Gibbs free energy difference per unit volume of the phase of molecular volume V condensed from the supersaturated vapor of pressure 'P' to the equilibrium pressure  $P_e$  ( $P/P_e = S$  is supersaturation). The radius of the critical nucleus ( $r^*$ ) which has maximum Gibbs free energy is given by and corresponding Gibbs free energy ( $\Delta G^*$ ) in terms of various surface energies is given by

$$r^* = 2\sigma_{cv}/\Delta G_v = 2\Delta G_v V / (kT \ln(P/P_e)) \quad (1.4)$$

$$\Delta G^* = 16/3\pi\sigma_{cv}/\Delta G_v \phi(\theta) \quad (1.5)$$

Where  $\phi(\theta) = \frac{1}{4}(2 - 3\cos\theta + \cos^3\theta)$

$\theta$  is contact angle in a condensate(c)-vapor(v)-substrate(s) system[12].

The nucleation rate  $I$  is proportional to the product of the concentration  $N^* = N_0 \exp(\Delta G^* / kT)$  of the critical nuclei and the rate  $\Gamma$  at which molecules join the critical nuclei by diffusion process.

$$I = Z(2\pi r^* \sin\theta) \Gamma N^* \quad (1.6)$$

$Z$  is Zeldovich correction factor.

Thus one can control the nucleation rate by controlling the deposition parameters such as temperature and deposition rate i.e impingement of flux which intern controls the morphology and growth of the film.

Once the randomly distributed, three dimensional nuclei are formed, rapidly approaches a saturation density with small amount of deposit. These nuclei then grow to form island whose shapes are determined by interfacial energies and deposition condition. The growth is diffusion controlled [13-15]. As an island increase their size by further deposition and come close to each other, the larger ones appear to grow by coalescence of the smaller ones. Island density decreases continuously and its rate is determined by deposition conditions. The coalescence phenomena have a profound effect on structure and properties of resultant film since recrystallization, grain growth, orientation changes, incorporation and removal of defects take place as a consequences of coalescence.

### 2.1 Experimental

The magnesium films were deposited using Hind HIVAC 12A 4D vacuum deposition system by resistive evaporation technique. To deposit the magnesium film, the magnesium powder (99% Pure, Merck) was placed in a molybdenum boat. The powder was then evaporated by resistive heating of the boat. During evaporation the pressure inside the chamber was maintained below  $10^{-5}$  mbar. Glass and  $Al_2O_3$  (alumina) substrates were used for deposition. The films with different thickness were deposited. i.e. 100, 200, 300 and 400 nm. However 300 nm

thick films were chosen for further experimental work. The deposition rates and thicknesses of the films were measured and controlled using digital quartz crystal deposition rate controller and monitor (DTM 101 operated at 6 MHz). The photograph and schematic of experimental set-up used for the deposition of magnesium films is shown in fig. 3.1

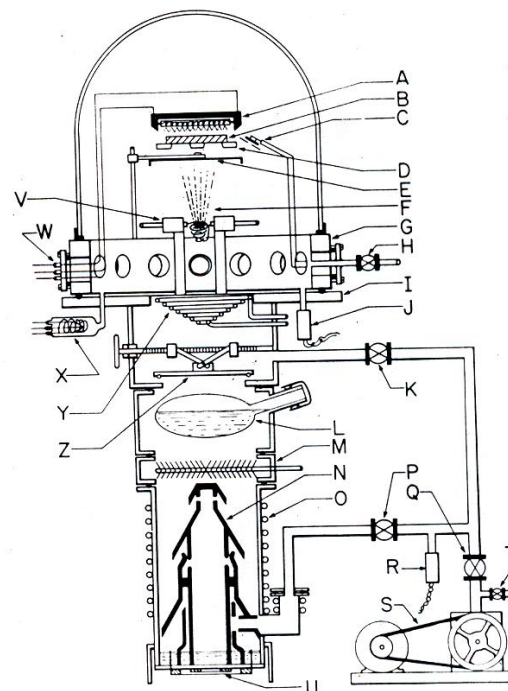


Fig. 3.1 Schematic of Experimental Set-up for deposition of magnesium films (the notations stands for A: Quartz iodine lamp heater, B: Substrate mask, C: Quartz crystal deposition rate controller and monitor, D: Substrates, E: Shutter, F: Source, G: Gasket, H: Air inlet valve, I: Base plate flange, J: Pirani or thermocouple gauge, K: Roughing valve, L: Liquid nitrogen trap, M: Cooled chevron baffles, N: Diffusion pump, O: Cooling coils, P&Q: Backing valve, R: Pirani gauge, S: Rotary pump with air inlet valve T, U: diffusion pump heater, V: Filament holder, W: multiple feed through, X: Ionization gauge, Y: Meissner trap, Z: Baffle valve

### 2.1 Substrate Cleaning

Glass and  $Al_2O_3$  substrates must be thoroughly cleaned before deposition and a variety of procedures exist for this purpose. The following procedure is used for cleaning of the substrates. The contaminants are first removed by lukewarm,

ultrasonically agitated, ionic detergent. The substrates are rinsed thoroughly several times in de-ionized water and latter subjected to a vapour digresser using pure alcohols. The cleaned substrates are stored/ immersed in pure alcohol and occasionally agited ultrasonically before use.

### 3. Results and discussion

#### 3.1 Growth of magnesium thin films on glass substrate.

The influence of the deposition parameters on film growth may be understood in terms of their effects on sticking coefficient, the nucleation density and surface mobility of adatoms. We have studied the effect of deposition rate on the growth of the magnesium film. As required the thickness of the magnesium films was kept constant (300 nm) for each deposition and vacuum of  $10^{-5}$  mbar was kept inside the chamber. The deposition of magnesium film was carried at various deposition rates such as  $10\text{\AA}/\text{sec}$ ,  $20\text{\AA}/\text{sec}$ ,  $35\text{\AA}/\text{sec}$  and  $50\text{\AA}/\text{sec}$  on glass substrates. These films are then characterized by x-Ray diffraction technique. Fig. 3.2 (a-d) shows the XRD pattern of the films deposited at the deposition rates  $10\text{\AA}/\text{sec}$ ,  $20\text{\AA}/\text{sec}$ ,  $35\text{\AA}/\text{sec}$  and  $50\text{\AA}/\text{sec}$ . The well agreement of observed 'd' values of these films with JCPDS data (Card No.35-0821) confirms its hexagonal structure. From figure, it is clear that all the films show reflection along (002) plane revealing its c-axis orientation. However, films deposited at deposition rate  $10\text{\AA}/\text{sec}$ ,  $20\text{\AA}/\text{sec}$ ,  $35\text{\AA}/\text{sec}$  and  $50\text{\AA}/\text{sec}$  show minor reflections along (101) plane. The maximum crystallinity and maximum crystallite size of 132 nm was found for the film deposited at the deposition rate  $20\text{\AA}/\text{sec}$ . The obtained films were pinhole free and well adherent to substrate. Hence the deposition rate of  $20\text{\AA}/\text{sec}$  was found to be optimum for the nucleation of magnesium vapor atoms or cluster and its subsequent growth into continuous magnesium film. Films deposited at the deposition rate lower than  $20\text{\AA}/\text{sec}$  shows pinholes due to insufficient impingement of flux of vapor atoms to form required super saturation to have required nucleation density to form a cluster for its further growth. Also deposition rate higher than  $20\text{\AA}/\text{sec}$  yields films, which are non adherent to the substrate. At higher deposition rate, the rate of

impingement of vapor atoms is higher than ad atom diffusion rate which disturbs the equilibrium resulting in poor quality film. Further increase in deposition rate than  $35\text{\AA}/\text{sec}$  produces the films, which are non adherent as well as with pinholes.

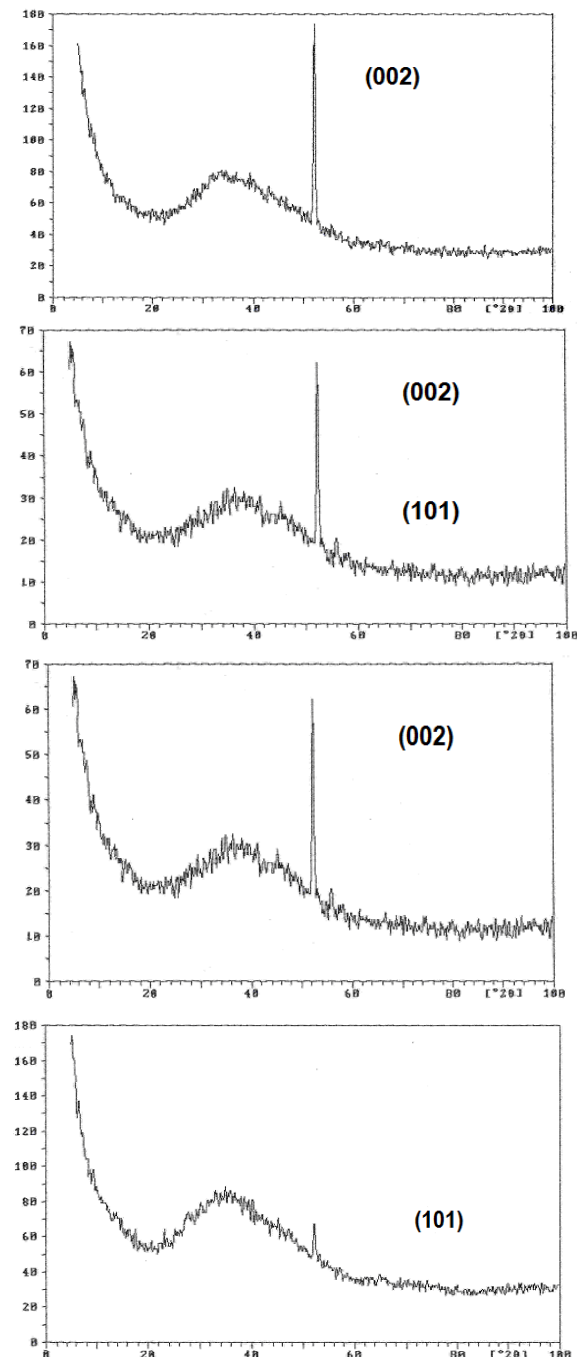


Fig. 3.2 XRD Pattern of vacuum deposited magnesium film on glass substrate with deposition rate  $10\text{\AA}/\text{sec}$ ,  $20\text{\AA}/\text{sec}$ ,  $35\text{\AA}/\text{sec}$  and  $50\text{\AA}/\text{sec}$ .

Further the crystallite size was calculated using Debye Scherrer's formula for crystallite size [16]

$$t = \frac{0.9\lambda}{\beta \cos \theta_B} \quad (3.7)$$

Where, t = particle size,  $\theta_B$  = diffraction angle,  $\lambda$  = wavelength of x-rays and  $\beta$  is line broadening at Full Width at Half Maxima (FWHM)

Crystallite size of a vapor deposited polycrystalline magnesium films increases with increase in deposition rate. This increase in crystallite size is not indefinite but after a saturation value of deposition rate the crystallite size begins to decrease rapidly. The effect of deposition rate on the film growth is tabulated in table 3.1

Table.3.1 Effect of deposition rate on the film growth

| Deposition rate $\text{\AA}/\text{sec}$ | Crystallite size nm | Adherence to substrate | Quality of film |
|---|---------------------|------------------------|-----------------|
| 10                                      | 65 $\pm$ 3          | Adherent               | Pinholes        |
| 20                                      | 132 $\pm$ 5         | Adherent               | Pinhole free    |
| 35                                      | 73 $\pm$ 2          | Non adherent           | Pinhole free    |
| 50                                      | 54 $\pm$ 2          | Non adherent           | Pinholes        |

The deposition rate of 20  $\text{\AA}/\text{sec}$  yields good quality, well adherent and pinhole free films. Here film adherence is concerned with the ability of the film to remain intact during soft electrochemical synthesis of  $\text{MgB}_2$  from non-aqueous bath, DMSO and pinholes are observed through Metzger optical microscope and Scanning electron Microscope (JEOL 6360). The optimized parameters for deposition of c-axis oriented magnesium films on glass substrates are tabulated in table 3.2.

Table.3.2 Optimized deposition parameters for the deposition of magnesium films on glass substrates.

| Parameter          | Optimized value            |
|--------------------|----------------------------|
| Deposition rate    | 20 $\text{\AA}/\text{sec}$ |
| Pressure           | 10 <sup>-5</sup> mbar      |
| Thickness          | 300 nm                     |
| Growth temperature | Room Temperature           |

The morphological studies of the vacuum deposited magnesium films were carried out by using Scanning Electron Microscope (SEM). Fig. 3.3 shows SEM images of magnesium films grown on glass substrate by vacuum evaporation technique at the deposition rate of (a & b) 10  $\text{\AA}/\text{sec}$ , (c & d) 20  $\text{\AA}/\text{sec}$ , (e & f) 35  $\text{\AA}/\text{sec}$ . The film deposited at deposition rate 20  $\text{\AA}/\text{sec}$  shows smooth pinhole free surface. However, the films deposited at the deposition rate 35  $\text{\AA}/\text{sec}$  show pinholes.

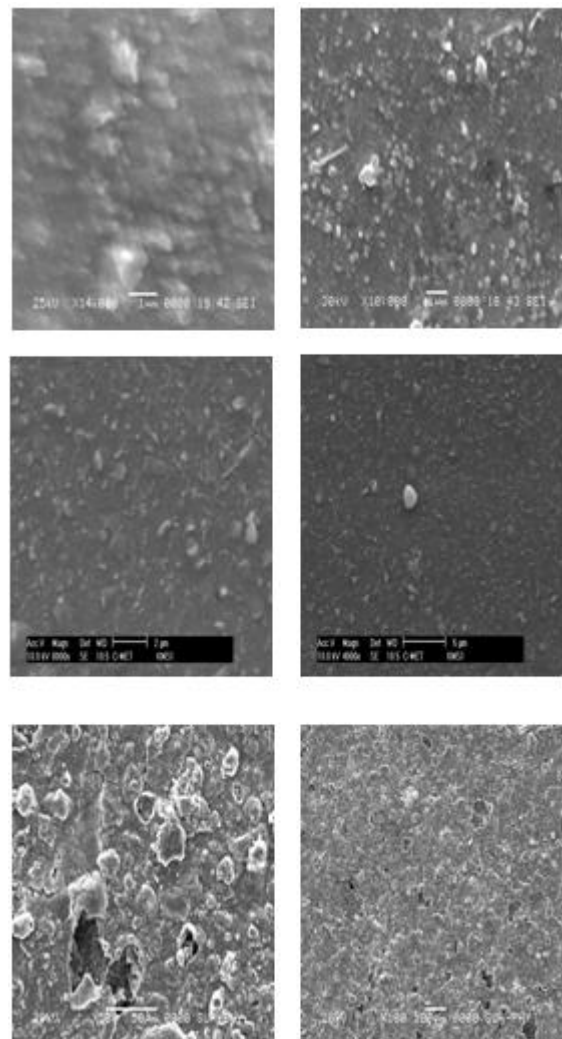


Fig. 3.3 SEM image of vacuum deposited magnesium films on glass substrate with deposition rate of (a & b) 10  $\text{\AA}/\text{sec}$ , (c & d) 20  $\text{\AA}/\text{sec}$ , (e & f) 35  $\text{\AA}/\text{sec}$ .

Further, surface morphology and surface roughness of the film deposited on glass substrate were examined by Atomic Force Microscope (AFM). Fig. 3.4 shows 3D and 2D AFM images of vacuum

deposited magnesium film on glass substrate at deposition rate  $20 \text{ \AA} / \text{sec}$ . It reveals smooth and fine grain surface of the magnesium film. The surface roughness calculated for this film is of the order of  $25 \text{ nm}$ .

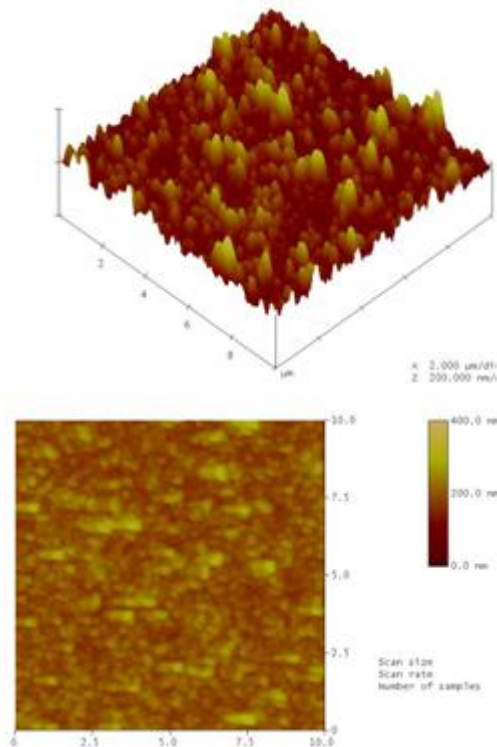


Fig. 3.4 The 3D and 2D Atomic Force Microscope (AFM) image of vacuum deposited magnesium film deposited on glass substrate at deposition rate  $20 \text{ \AA} / \text{sec}$

### 3.5.2 Growth of magnesium thin films on $\text{Al}_2\text{O}_3$ substrate

For the growth of magnesium films by physical vapor deposition method, the sticking coefficient of magnesium is low [17], which makes the required optimized deposition rate much higher at about  $20 \text{ \AA} / \text{s}$  for the growth of magnesium film on amorphous glass substrate. This results in the film growth with lower crystallinity. Moreover, the use of crystalline  $\text{Al}_2\text{O}_3$  substrates, having closer 'd' values to that of magnesium was expected to yield improved crystallinity for the growth of magnesium films relatively at lower deposition rate. The XRD studies were carried out to examine the growth of magnesium films on  $\text{Al}_2\text{O}_3$  substrates. Fig. 3.5 shows the X-ray diffraction pattern of the magnesium film

on  $\text{Al}_2\text{O}_3$  substrates deposited at deposition rate  $10 \text{ \AA} / \text{s}$ . It shows reflections of the planes (002), (101), (110), (200), (201), (202), (104) and (210) corresponding to magnesium along with substrate ( $\text{Al}_2\text{O}_3$ ) peaks. Most of the high intensity peaks corresponding to magnesium are much closer to substrate (as shown in inset of fig.3.5) peaks indicating the preferred orientation of the magnesium grains along that of substrate planes. Hence, in contrast to films on glass substrates the magnesium films deposited on  $\text{Al}_2\text{O}_3$  substrates are not c-axis oriented. However, the films showed the improved crystallinity. This variation in orientation, which results change in stress originated in the magnesium films grown, is extremely important for the superconducting properties of the  $\text{MgB}_2$  films. Blumberg et.al [18] have grown tin (Sn) films on glass substrate both with c-axis normal to the plane of the film and c axis parallel to the plane of the film. They found that the critical temperature of the films depends upon stress arising when they are constrained to follow the contraction of the soda lime glass on cooling to low temperature. The stress in the film (Sn) and the critical temperature vary according to the direction of the tetrad axes. When the tetrad axes is normal to the plane of the film the stress are small (the diad axes in the plane of the film make fairly well thermal contraction of the substrate). With this orientation, the change in critical temperature is only 0.01 to 0.02 K above the bulk value. While for tetrad axis parallel to the plane of the film, this change is 10 to 20 times larger than for former case. This indicates the orientation of the film grown and hence originated stress does affect the superconducting properties like  $T_c$  values.

The crystallite size calculated by Debye Scherrer formula, for the magnesium film deposited at deposition rate  $10 \text{ \AA} / \text{s}$  on  $\text{Al}_2\text{O}_3$  substrates was found to be  $224 \text{ nm}$  which is much higher than that observed for the film on glass substrate. Further, fig. 3.6 shows the X-ray diffraction pattern of the magnesium film on  $\text{Al}_2\text{O}_3$  substrates deposited at deposition rate 5 and  $15 \text{ \AA} / \text{s}$ . It shows reflections of the planes (002), (110), corresponding to magnesium along with substrate ( $\text{Al}_2\text{O}_3$ ) peaks. The XRD pattern reveals that the deposition rate does

not affect much the growth of magnesium film on  $Al_2O_3$ . However, the films deposited at deposition rate  $10 \text{ \AA/s}$  are comparatively adhesive to substrate. The optimized deposition parameters for the deposition of magnesium films on  $Al_2O_3$  substrates are listed in table.3.3.

Table.3.3 Optimized deposition parameters for the deposition of magnesium films on  $Al_2O_3$  substrates.

| Parameter          | Optimized value        |
|--------------------|------------------------|
| Deposition rate    | $10 \text{ \AA/sec}$   |
| Pressure           | $10^{-5} \text{ mbar}$ |
| Thickness          | 300 nm                 |
| Growth temperature | Room Temperature       |

Further fig. 3.5 shows SEM image of magnesium film deposited on  $Al_2O_3$  substrates. SEM image reveals that there is well development of grains corresponding to the magnesium compared to the film deposited on glass substrate.

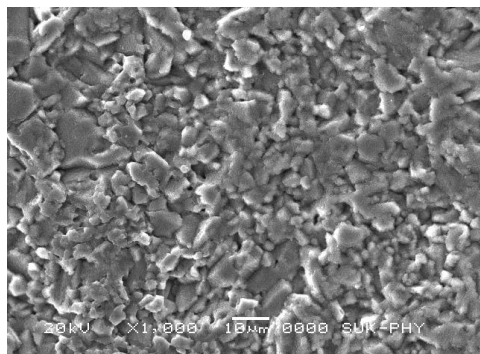


Fig. 3.5 SEM image of vacuum deposited magnesium film on  $Al_2O_3$  substrate with deposition rate of  $10 \text{ \AA/sec}$

### 3.6 Conclusions

The magnesium films were grown on glass and  $Al_2O_3$  substrates by vacuum evaporation technique. The effect of deposition rate on growth of the magnesium film was studied and found that the film deposited at deposition rate  $20 \text{ \AA/sec}$  on glass substrate yields c-axis oriented magnesium films. This is confirmed by XRD studies which shows single peak of (002) for the film grown at  $20 \text{ \AA/sec}$ . However, the film grown at the deposition rate other than  $20 \text{ \AA/sec}$  show minor peak of (101) plane.

The film grown on  $Al_2O_3$  substrates yields films with higher crystallinity which was confirmed by XRD and SEM studies. The optimized deposition

rate for growth of magnesium films on  $Al_2O_3$  substrates is  $10 \text{ \AA/s}$ . The improved crystallinity of the film on  $Al_2O_3$  substrates is due to crystallinity of  $Al_2O_3$  substrates compared to amorphous glass substrate.

### References

- [1]. Thin Film Phenomena-Kasturi L Chopra, Ch II, Mcgraw Hill book Company 1969
- [2]. Basset G A, Phil. Mag. 3 (1958)1042
- [3]. Basset G A, Menter J W, and Pashley D W, Proc. Roy. Soc. London, A246 (1959) 345
- [4]. Thin Film Phenomena-Kasturi L Chopra, Ch IV, Mcgraw hill book Company 1969
- [5]. Langmuir I, Phy. Rev. 8(1916)149
- [6]. N Cabrera, Discussions Faraday Soc.28 (1959) 16
- [7]. Volmer M and Weber A, Z. Phys. Chem, 119 (1925) 277
- [8]. Becker R and Doring W, Ann. Physik. 24(1935) 719
- [9]. Holomon J H and Tarnbull D, Prog. Metal Phys. 4 (1953) 333
- [10]. Pound G M, Simnad M T and Yang L, J. chem. Phys. 22 (1954) 1215
- [11]. Hirth G P and Pound G M, Nucleation and Growth Kinetics, "Condensation and Evaporation", The Macmillan Company New York. 1663
- [12]. Chakraverty B K and Pound G M Acta Mat. 12 (1964) 851
- [13]. Kuczynski G S, Trans AIME 185 (1949)169
- [14]. Kingery W D and Berg M, J. Appl. Phys. 26 (1955) 1205
- [15]. Nichols F A, J. Appl. Phys., 37 (1966) 2805.
- [16]. Cullity B D, Elements of X-ray Diffraction, Addison Wesley, Readorig Massachusetts
- [17]. Zi-Kui Liu and D.G. Schlom, Appl. Phys.Lett. 78 (23) (2001) 3678
- [18]. R. H. Blumberg and D. P. Seraphim, J. App. Phys. 33 (1) (1962) 163